

A Paper-Based Wearable Photodetector for Simultaneous UV Intensity and Dosage Measurement

Sa Cai, Chaolei Zuo, Jiayu Zhang, Hui Liu, and Xiaosheng Fang*

Photodetectors, which convert the light signal into other forms of signal, have been under the spotlight of research for many years because they are widely applied in monitoring, communication, and imaging. Most of the currently available photodetectors can output electrical signals to indicate the transient light intensity, while some display color change to reveal the absorbed light dosage. However, there is no device that can tell the transient light intensity and accumulated light dosage at the same time. Here, a paper-based wearable photodetector that can simultaneously measure transient light intensity and accumulated light dosage is reported. The phosphomolybdic acid/citric acid system, whose color change can be observed by the naked eye, is designed as the photochromic material to combine with photodetective materials (using 2D $\text{Sr}_2\text{Nb}_3\text{O}_{10}$ and ZnO nanoparticle as examples) on paper. Such paper-based photodetector fully utilizes natural hygroscopicity and softness of paper, showing decent flexibility. Its optoelectronic signal remains stable even after 1000 cycles of bending. To the best of one's knowledge, this is the first photodetector that can tell light intensity and dosage simultaneously. This work introduces a new type of wearable photodetector by structure design and material selection, shedding light on more novel works for convenient and practical photodetection.

1. Introduction


Ultraviolet (UV) light, whose wavelength ranges from 100 to 400 nm,^[1] is a double-edge sword to human beings. On one hand, UV light, which is an important component of natural sunlight, is harmful to humans.^[2–4] As widely acknowledged, UV light can negatively affect human skin, leading to burning and canceration.^[5–7] On the other hand, UV light is extensively used in industry, research, and life.^[8–11] For instance, UVC is one of the simplest and the most effective methods for disinfection under the breakout of Covid-19. It has been reported that UVC irradiation effectively inactivates SARS-CoV-2 virus (Figure S1, Supporting Information).^[12] 375 J m⁻² UVC (280 nm) irradiation can kill 99.9% SARS-CoV-2 virus. In addition, UV light has found its way into monitoring, communication,

and imaging in modern society.^[13–15] Therefore, making the best use of UV light to serve us humans has become one of the hottest topics in research. To date, various kinds of photodetectors have been designed and fabricated to detect UV light.^[16–19] Among them, photodetectors that measure the transient UV intensity are the major types and they are typically what scholars refer to when they mention photodetectors.^[20–22] These types of photodetectors transform light signal into electronic signals, outputting a larger current as the light intensity increases.^[23,24]

Apart from photodetectors that monitor the transient light intensity, photochromic materials that change color when a certain amount of light is absorbed are another kind of photodetectors and they serve for absorbed dosage measurement.^[25–28] Such materials include organic materials,^[29,30] metal oxide,^[31,32] polyoxometalates,^[33] etc.^[26] In the past few years, practical applications based on photochromic material are emerging.^[34–37] Zou et al. manufactured a skin-color-specific and spectrally selective naked-eye dosimetry of UVA, UVB, and UVC radiations, which was based on the reaction between phosphomolybdic acid (PMA) and lactic acid under UV illumination.^[38] By covering polymer films on the photochromic material, they were able to decrease the sensitivity of the dosimetry to meet the needs of different skin types as well as quantify the UV dosage. Other researchers have also used smartphone camera for UV dosage analysis.^[39]

With the prosperous development of photodetectors, however, no single photodetector that can measure the transient light intensity and accumulated light dosage at the same time has been reported. Here, we designed a paper-based photodetector that can achieve the simultaneous recording of UV intensity and dosage while demonstrating decent flexibility. The device skillfully utilized the natural hygroscopicity and softness of paper by combining PMA/citric acid photochromic system with semiconductor materials ($\text{Sr}_2\text{Nb}_3\text{O}_{10}$ nanosheets and ZnO nanoparticles were chosen as examples) in a designed structure. PMA/citric acid photochromic system is responsible for dosage measurement and the semiconductor material is for the transient light intensity recording. The PMA/citric acid photochromic system, which was reported for the first time, was more sensitive and stable than the previous reported PMA/lactic acid photochromic system and served as a strong candidate for

S. Cai, C. L. Zuo, J. Y. Zhang, Dr. H. Liu, Prof. X. S. Fang
Department of Materials Science
Fudan University
Shanghai 200433, P. R. China
E-mail: xshfang@fudan.edu.cn

 The ORCID identification number(s) for the author(s) of this article can be found under <https://doi.org/10.1002/adfm.202100026>.

DOI: 10.1002/adfm.202100026

UV dosimetry. For the semiconductor material, we can choose different materials to meet different needs and here, we demonstrated $\text{Sr}_2\text{Nb}_3\text{O}_{10}$ and ZnO as examples. By spray coating semiconductor material and painting the photochromic solution on a piece of filter paper in a designed structure, we successfully achieved a wearable photodetector that can tell the transient light intensity and accumulated absorption at the same time. Since there is no direct contact between semiconductor material and photochromic material, the two materials will not interact with each other. When there is no UV light, the photodetector outputs a low current and shows no color change. When UV illumination is on, its current increases significantly and the photochromic material painted pattern gradually becomes blue, implying the light intensity and dosage. When the UV light is turned off afterward, the current decreases to the original level and the painted pattern remains blue.

2. Results and Discussion

2.1. Photochromic Material Synthesis and Characterization

Citric acid was selected as the electron donor in our photochromic system to reduce PMA under UV illumination to indicate the absorbed UV dosage. We first determined the

suitable concentration of PMA and citric acid so that the highest UV sensitivity could be achieved. 5×10^{-3} M PMA/ 300×10^{-3} M citric acid solution was proven to be the most suitable system for UV detection for it displayed the highest UV sensitivity with minimal raw material (Figure S2, Supporting Information) and all discussions later were based on this material system. The pristine solution of 5×10^{-3} M PMA/ 300×10^{-3} M citric acid was colorless and transparent. After absorbing UV light, the solution became blue and it remained stable after heating in oven at 70°C for 10 min (Figure 1b). The mechanism of the color change is a redox reaction. The color of the system was determined by the valence state of molybdenum ion in PMA. Mo^{6+} is colorless and Mo^{5+} is blue. The valence of Mo is +6 in the 5×10^{-3} M PMA/ 300×10^{-3} M citric acid solution. After absorbing UV, Mo^{6+} was gradually reduced to lower valence and PMA became a mixed-valence species, known as “heteropoly blues” and turned blue (Figure 1a).^[40,41] The accumulated dosage of UV greatly influences the extent of the redox reaction and as a result, this reaction can be used for UV dosage measurement.

Compared with the previous reported PMA/lactic acid photochromic system of the same concentration, PMA/citric acid system was more sensitive to UV dosage and more stable in dark environment. Figure S3 (Supporting Information) showed the photos of PMA/citric acid solution and PMA/lactic acid

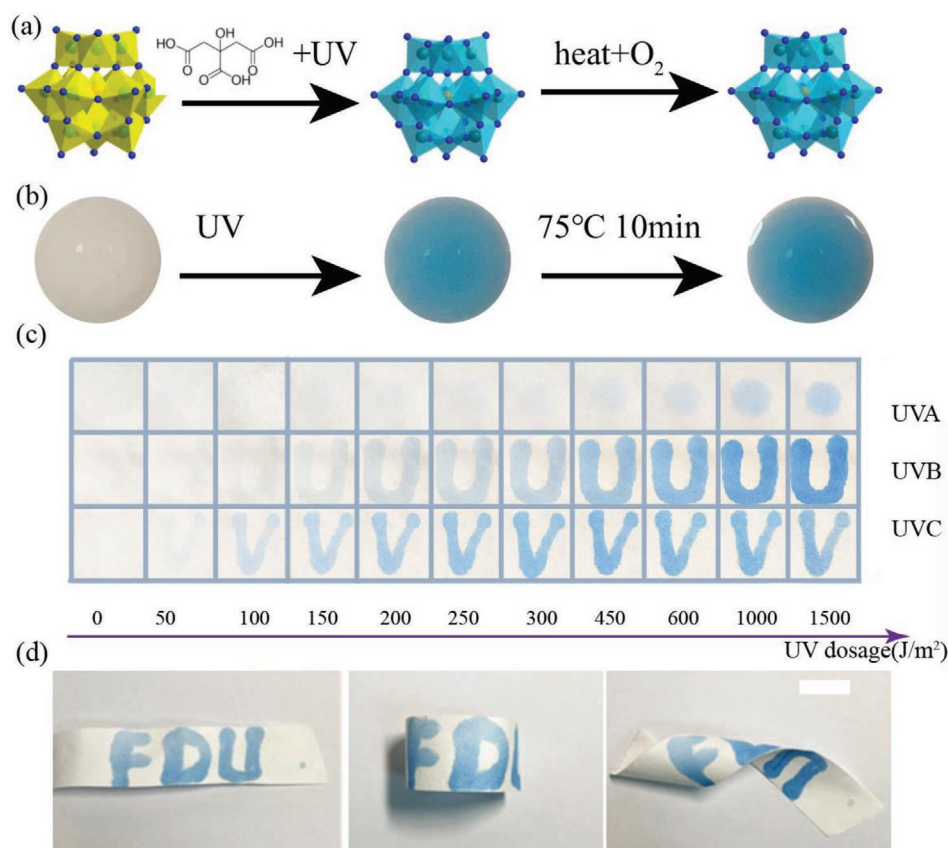


Figure 1. a) The photochromic mechanism of the PMA/citric acid under UV illumination. b) Photos of the initial 5×10^{-3} M PMA/ 300×10^{-3} M citric acid photochromic solution and that after UV illumination and heating. c) Photos of different patterns painted by the 5×10^{-3} M PMA/ 300×10^{-3} M citric acid photochromic solution system after absorbing different dosages of UV light (UVA: 365 nm, UVB: 310 nm, UVC: 254 nm). d) The flexibility of the paper-based photochromic system (scale bar: 1 cm).

solution after absorbing the same amount of UV light and they both changed from transparent to blue. It might be hard to tell the relative sensitivity from the color change of the solution. Therefore, a drop of each solution was dripped on a piece of filter paper and the color changes of two dried materials on the filter paper were compared. Figure S4 (Supporting Information) showed the distinct responsive difference of PMA/lactic acid and PMA/citric acid, where PMA/citric acid was much more sensitive to UV illumination. The long-term stability of PMA/citric acid system was also superior to that of PMA/lactic acid system. Figure S5 (Supporting Information) presented photos of a) the initial solution, b) solution kept in dark for 140 h, and c) solution kept in dark for 30 days. The PMA/citric acid system was still transparent even after 30 days in dark, while the PMA/lactic acid system gradually turned blue.

To quantify the sensitivity of PMA/citric acid solution to different types of UV light (UVA: 365 nm, UVB: 310 nm, and UVC: 254 nm), photos of solution were taken when the accumulated UV dosages were 0, 50, 100, 150, 200, 250, 300, 450, 600, 1000, and 1500 J m⁻². Figure 2a shows the collective of those photos and there was a difference on responsive sensitivity for

different UV lights. The PMA/citric acid system was sensitive to UVB and UVC light and was inert to UVA light. The transmittance spectrums of the solution after absorbing different UVA, UVB, and UVC dosages were plotted in Figure 2b–d, respectively. Change of transmittance under certain UV dosages as a function of wavelength was plotted in Figure S6 (Supporting Information). It could be observed that the transmittance at around 650 nm varied the most as the solution absorbing more UV light, while the transmittance at a longer wavelength varies more when the absorbed UV dosage was low. The transmittance value at 650 nm was collected from Figure 2b–d and was plotted in Figure 2e, where an obvious discrepancy between UVA and UVB/UVC could be found. Absorbance spectrums of the pristine PMA/citric acid solution and solution after different UV absorptions were shown in Figure S7 (Supporting Information). It confirmed that PMA/citric acid photochromic system was less sensitive to UVA compared with UVB and UVC.

The photochromic solution was then used as the ink to write different patterns on a piece of filter paper. Photos were taken when the accumulated UV dosages were 0, 50, 100, 150, 200, 250, 300, 450, 600, 1000, and 1500 J m⁻² for three wavelengths

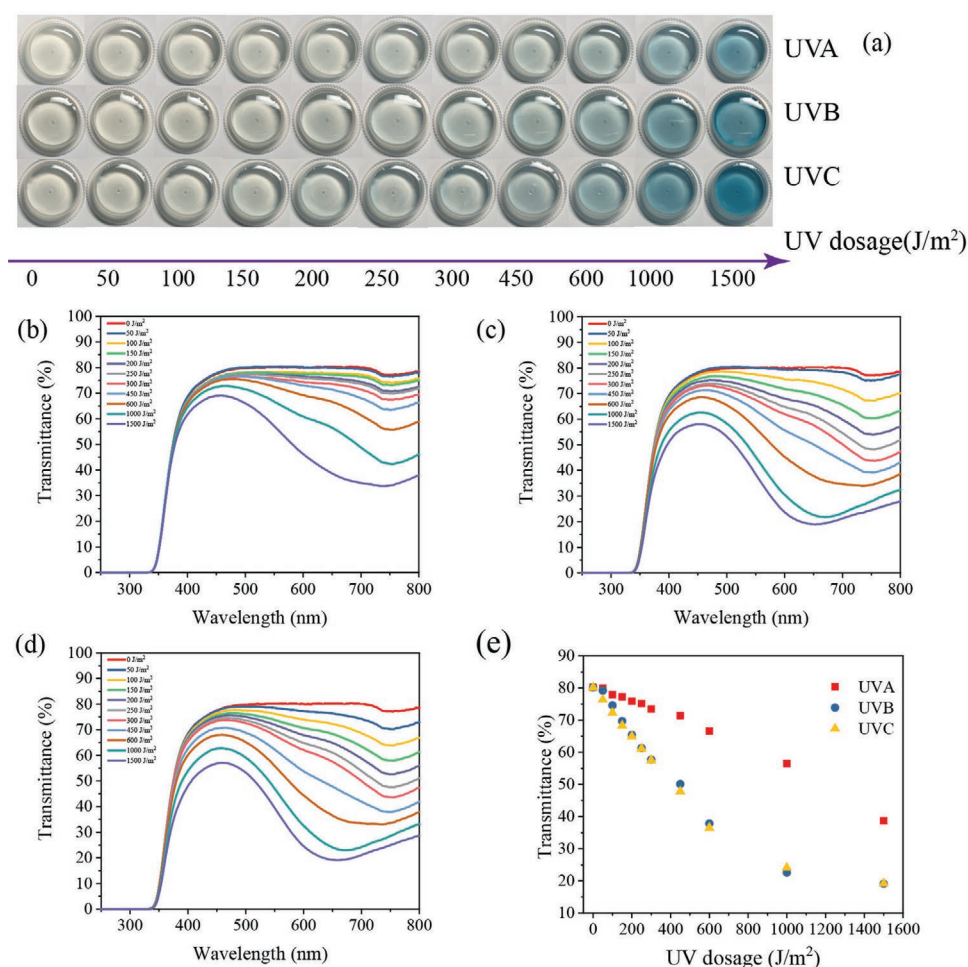


Figure 2. a) Photos of 5×10^{-3} M PMA/ 300×10^{-3} M citric acid photochromic solution after absorbing different dosages of UV light (UVA: 365 nm, UVB: 310 nm, UVC: 254 nm). The transmittance spectrum of 5×10^{-3} M PMA/ 300×10^{-3} M citric acid photochromic solution after absorbing different dosages of b) UVA, c) UVB, d) UVC. e) The transmittance value at 650 nm for 5×10^{-3} M PMA/ 300×10^{-3} M citric acid photochromic solution after absorbing different dosages of UV light.

(UVA: 365 nm, UVB: 310 nm, and UVC: 254 nm), as shown in Figure 1c. The distinction in sensitivity was more obvious when the material was written on paper. Such a differentiating ability is of vital importance in practice because of the following reasons. First, UVC is quite limited in nature because it is absorbed by ozone layer and cannot reach the earth. Thus, it does not matter that this system demonstrated limited differentiation between UVB and UVC. Second, UVB and UVA play different roles in affecting human health. Hence, distinguishing UVA and UVB is of crucial importance and it is exactly what PMA/citric acid system could achieve. Third, the photochromic ability enables the system to detect UVC under some special circumstances such as UVC disinfection systems to avoid possible accidents. Tragedies such as kindergarten kids were hurt by UV lamps could be avoided. In conclusion, PMA/citric acid was an efficient photochromic system to measure the accumulated UV dosage and could differentiate UVA between UVB and UVC. Furthermore, by adjusting the material concentration in the system, we can easily reduce the UV sensitivity of the system to meet different needs, as shown in Figure S2 (Supporting Information).

Apart from the better accessibility to naked eyes, another advantage of applying the photochromic material as ink is that it utilized the natural hygroscopicity and softness of paper, thus making the paper-based device flexible and wearable. Figure 1d showed the “FDU” pattern photochromic material on paper, which can be twisted and folded. With the high-sensitive UV photochromic material for dosage measurement on hand, we want to combine the PMA/citric acid system with UV intensity sensing material to achieve an integrated photodetector for simultaneous UV dosage and intensity measurement.

2.2. Semiconductor Material Characterization

2D $\text{Sr}_2\text{Nb}_3\text{O}_{10}$ nanosheets, which was first reported as a UV sensing material by our group^[42] and has a bandgap of ≈ 3.9 eV,

was selected as the photodetective material due to its strong response to UV light and its blindness to visible light. The two-step synthesized nanosheets were spray-coated onto a piece of filter paper on a 150 °C hot plate to form a compact film (Figure S8, Supporting Information). Ag paste was then used as the electrodes to construct a metal–semiconductor–metal photodetector. The scanning electron microscopy (SEM) image of the sprayed $\text{Sr}_2\text{Nb}_3\text{O}_{10}$ nanosheets was shown in Figure 3a, revealing the compact structure of the film and guaranteeing the quality of the constructed photodetector. Figure 3b presented the SEM image of sparse $\text{Sr}_2\text{Nb}_3\text{O}_{10}$ nanosheets in high resolution, showing the size of the nanosheets. The UV–vis spectrum (Figure 3c) confirmed the wide bandgap of 2D $\text{Sr}_2\text{Nb}_3\text{O}_{10}$, indicating its advantage as a solar-blind UV sensor. Optoelectronic properties of the spray-coated $\text{Sr}_2\text{Nb}_3\text{O}_{10}$ nanosheets on the filter paper were characterized by Keithley 4200-SCS. Figure 3d showed the I – V characteristics from -5 to 5 V in dark, under 260, 310, and 360 nm illuminations. The correspondent I – T curves under 5 V external bias were shown in Figure 3e. The dark current was 1.6×10^{-8} A and the photocurrent was 6.9×10^{-6} , 2.5×10^{-5} , and 1.7×10^{-6} A under 360, 310, 260 nm, respectively, for the $\text{Sr}_2\text{Nb}_3\text{O}_{10}$ nanosheet film. The light-to-dark current ratio was 4.3×10^2 , 1.6×10^3 , and 1.1×10^2 for UVA (360 nm, 2.5 mW cm^{-2}), UVB (310 nm, 1.6 mW cm^{-2}), and UVC (260 nm, 0.46 mW cm^{-2}), respectively.

The I – T characterization of the paper-based $\text{Sr}_2\text{Nb}_3\text{O}_{10}$ nanosheet film under light of different wavelengths was shown in Figure S9 (Supporting Information). According to the expression of responsivity^[43]

$$R_\lambda = \frac{I_{\text{ph}} - I_{\text{d}}}{PS} \quad (1)$$

where I_{ph} is the photocurrent, I_{d} is the dark current, P is incident illumination power density, and S is the effective illumination area. The calculated responsivity of $\text{Ag}/\text{Sr}_2\text{Nb}_3\text{O}_{10}/\text{Ag}$

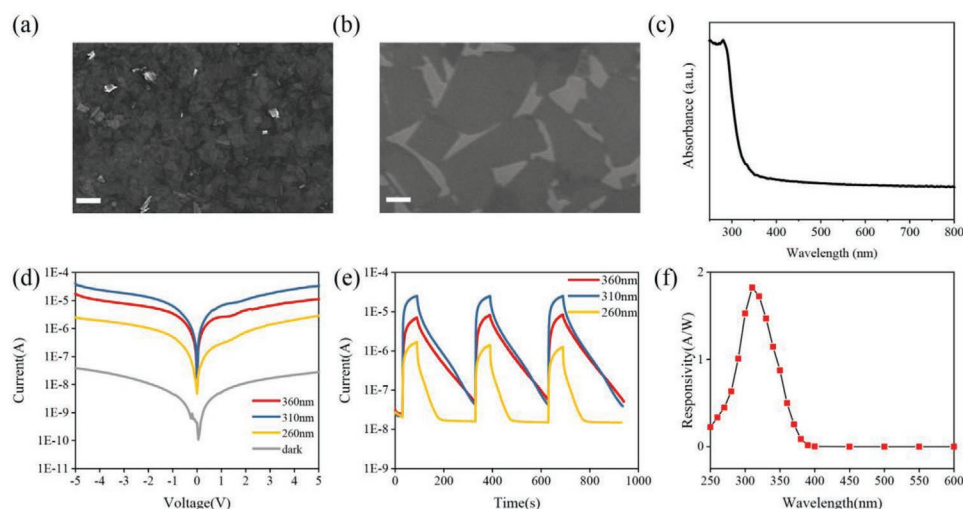


Figure 3. a) The SEM image of the $\text{Sr}_2\text{Nb}_3\text{O}_{10}$ nanosheets (scale bar: 1 μm), indicating its compact structure. b) The SEM image of the sparse $\text{Sr}_2\text{Nb}_3\text{O}_{10}$ nanosheets (scale bar: 200 nm), indicating the size of single nanosheet. c) The UV–vis spectrum of $\text{Sr}_2\text{Nb}_3\text{O}_{10}$ nanosheets, showing its strong absorption in the UV range. d) The I – V characterization of $\text{Sr}_2\text{Nb}_3\text{O}_{10}$ nanosheets for UVA, UVB, and UVC lights. e) The I – T characterization of $\text{Sr}_2\text{Nb}_3\text{O}_{10}$ nanosheets for UVA, UVB, and UVC lights. f) The responsivity of the $\text{Sr}_2\text{Nb}_3\text{O}_{10}$ nanosheet, showing its selective response to UV light.

was plotted in Figure 3f, where it peaked 1.8 A W^{-1} around 310 nm. The responsivity plot clearly showed the blindness of $\text{Sr}_2\text{Nb}_3\text{O}_{10}$ to visible light, assuring its superiority as a UV sensing material. The large photocurrent and decent responsivity are advantages of $\text{Sr}_2\text{Nb}_3\text{O}_{10}$, while its slow response speed remains to be a defect. In Figure 3e, the dark current even failed to decrease to the initial level when the illumination light was 360 and 310 nm. If more time was given, the dark current after longer wavelength illumination could decrease to the same level of that after 260 nm illumination (Figure S10, Supporting Information).

Therefore, we chose another semiconductor material, ZnO, as our potential candidate for dual-functional device. We utilized the commercial ZnO nanoparticle by dissolving it in deionized (DI) water. ZnO suspension was then spray-coated on a piece of filter paper like $\text{Sr}_2\text{Nb}_3\text{O}_{10}$ nanosheets and its UV-vis spectrum was shown in Figure S11 (Supporting Information). The SEM image revealed the compact structure of ZnO on

the filter paper (Figure S12, Supporting Information). The I - V characterization for UVA, UVB, and UVC, I - T characterization for UVA, UVB, and UVC, I - T characterization under light of different wavelengths and its calculated responsivity were given in Figures S13–S16 (Supporting Information), respectively. The photocurrent of ZnO was lower than that of $\text{Sr}_2\text{Nb}_3\text{O}_{10}$, but its response speed was remarkably faster.

2.3. Paper-Based Device for Simultaneous UV Intensity and Dosage Measurement

We then spray-coated the $\text{Sr}_2\text{Nb}_3\text{O}_{10}$ nanosheet as the surrounding material on a piece of filter paper and then wrote a “UV” pattern on the center blank area using PMA/citric acid solution, as shown in Figure 4a, to fabricate the photodetector that can simultaneously measure the transient UV intensity and the accumulated UV dosage. Here, the spray coating technique showed

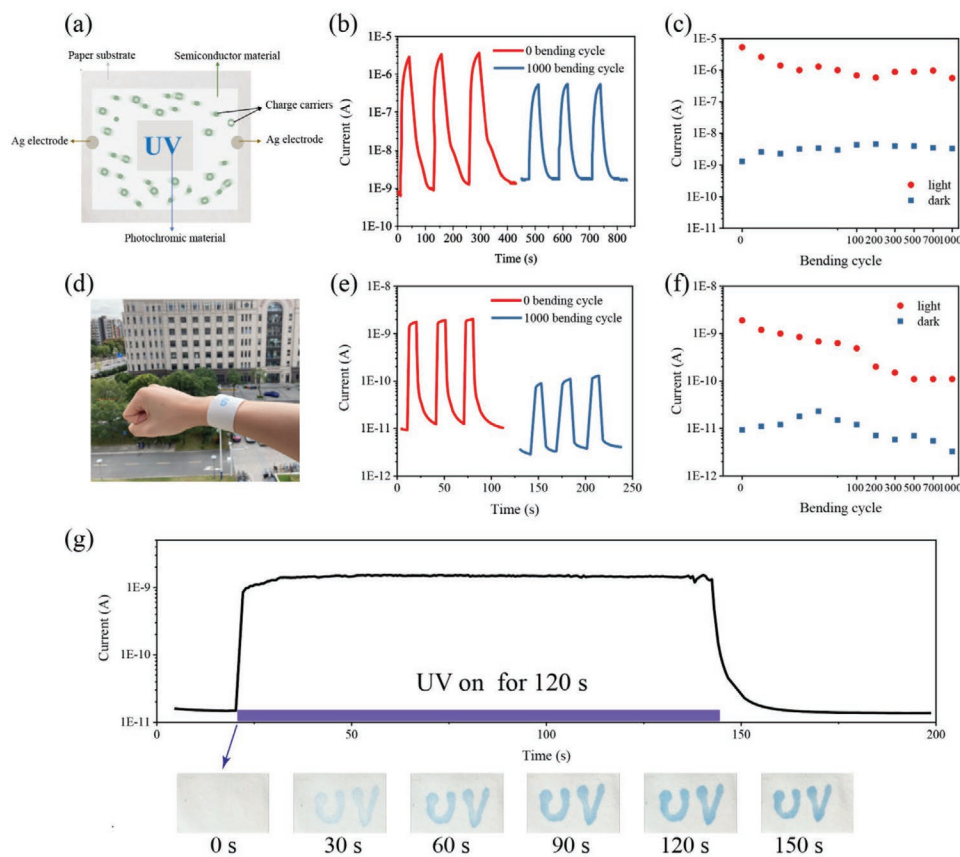


Figure 4. a) The schematic diagram of the final photodetector on a piece of filter paper: the light-gray area was spray-coated with photodetective material, where electrons (solid circles) and holes (hollow circles) would be generated and separated under external bias with UV illumination. The photochromic solution was used as ink to write the “UV” pattern in the center blank area of the filter paper, which would turn blue after absorbing UV light. There is no direct contact between semiconductor material and photochromic material. When UV light hit the device, this device could simultaneously output current to indicate the UV intensity and achieve color change to show the absorbed UV dosage. b) The I - T characterization of the whole device (using $\text{Sr}_2\text{Nb}_3\text{O}_{10}$ nanosheets as the photodetective material) before and after bending on the wrist for 1000 times. c) The dark current and photocurrent of the whole device (using $\text{Sr}_2\text{Nb}_3\text{O}_{10}$ nanosheets as the photodetective material) after 0, 1, 5, 10, 20, 50, 100, 200, 300, 500, 700, and 1000 times of bending. d) The photo of the final device on the human wrist. e) The I - T characterization of the whole device (using ZnO nanoparticle as the photodetective material) before and after bending on the wrist for 1000 times. f) The dark current and photocurrent of the whole device (using ZnO nanoparticle as the photodetective material) after 0, 1, 5, 10, 20, 50, 100, 200, 300, 500, 700, and 1000 times of bending. g) The output current and photos of the pattern of the final photodetector as UV light was on for 120 s. As UV light was turned on, the current surged and the “UV” pattern gradually turned blue. When the UV light was turned off, the current decreased but the pattern remained blue, still indicating the accumulated UV dosage.

a unique superiority. As the photochromic material and semiconductor material will affect the property of the other if there is direct contact between these two, we need to avoid such contact. Most depositing methods, including dip coating, will result in the diffusion of material when the substrate is paper. Spray coating on a hot plate perfectly addressed this issue. First, the velocity of flow is controllable and a small volume per second could be achieved. Second, the hot plate helps to evaporate water fast to minimize the water diffusion in paper.

The dried pristine device was colorless and looked like a simple piece of paper because the solution was transparent without any UV illumination and the $\text{Sr}_2\text{Nb}_3\text{O}_{10}$ nanosheets demonstrated little color. Figure S17 (Supporting Information) showed the spray-coated $\text{Sr}_2\text{Nb}_3\text{O}_{10}$ nanosheet film on a glass slide, which was transparent. When UV light hit the paper, the $\text{Sr}_2\text{Nb}_3\text{O}_{10}$ nanosheet film would generate an increased photocurrent to indicate the transient light intensity and the “UV” pattern would gradually turn blue for dosage indication as the redox reaction went on. When the UV illumination stopped, the current decreased to the original level and the “UV” pattern remained blue, indicating the accumulated UV dosage. Figure S18 (Supporting Information) showed the schematic diagram of the functioning photodetector. The flexibility of the integrated paper-based photodetector was also characterized. The device was bended on the wrist (Figure 4d) and its optoelectronic properties were measured before and after bending. Dark current and light current under 254 nm after different bending cycles were presented in Figure 4b,c. The device showed some fluctuation in currents when the bending cycle was less than 10. After 10 times bending, the currents remained relatively stable. The light-to-dark current ratio was 3.1×10^2 after 10 times bending. Even after 1000 times bending, the light-to-dark current ratio was as high as 1.7×10^2 . The optical images before and after 1000 bending cycles were given in Figure S19 (Supporting Information), where $\text{Sr}_2\text{Nb}_3\text{O}_{10}$ was tightly attached to the filter paper and no evident break could be found after 1000 bending cycles, explaining the decent optoelectronic properties after bending.

The construction method of such photodetector not only worked for $\text{Sr}_2\text{Nb}_3\text{O}_{10}$ nanosheets but was a general method. We demonstrated its universality by using ZnO nanoparticles as the photodetective material. ZnO was also used for constructing an integrated device like $\text{Sr}_2\text{Nb}_3\text{O}_{10}$ and its optoelectronic properties were measured before and after bending. Dark current and light current under 254 nm after different bending cycles were presented in Figure 4e,f. Compared with $\text{Sr}_2\text{Nb}_3\text{O}_{10}$ -nanosheet-based device, ZnO-nanoparticle-based device was less resistant to bending. Such a difference could be explained by its optical images before and after bending (Figure S20, Supporting Information). The initial ZnO film on filter paper was smooth. After 1000 bending cycles, some ZnO dropped, but there was still some attached to the filter paper, resulting in the decayed property. Figure 4g showed the current and color change of the final photodetector as UV light (254 nm) on and off.

3. Conclusion

In conclusion, a dual-functional paper-based wearable photodetector that can simultaneously measure the UV light intensity

and accumulated dosage was designed and fabricated using photochromic material (PMA/citric acid system) and semiconductor material ($\text{Sr}_2\text{Nb}_3\text{O}_{10}$ nanosheets and ZnO nanoparticle were used as examples). The final device utilized the natural hygroscopicity and softness of paper, and thus demonstrating decent flexibility. The skillful integration of photochromic material and photodetective material in this work demonstrated an elegant and universal method to fabricate new types of photodetectors and might inspire more creative work. Our future work will focus on the material improvement and the final goal is to fabricate a device that can wirelessly detect UV intensity and dosage at the same time and transfer the data to electronic devices for real-time monitoring.

4. Experimental Section

Selection of Citric Acid Concentration in the PMA/Citric Acid System: Stoichiometric PMA (Analytical Reagent) and citric acid (Analytical Reagent) were dissolved in DI water to form the photochromic system. Seven different concentrations of PMA/citric acid systems (1) 5×10^{-3} M PMA, 2) 5×10^{-3} M PMA + 10×10^{-3} M citric acid, 3) 5×10^{-3} M PMA + 50×10^{-3} M citric acid, 4) 5×10^{-3} M PMA + 100×10^{-3} M citric acid, 5) 5×10^{-3} M PMA + 200×10^{-3} M citric acid, 6) 5×10^{-3} M PMA + 300×10^{-3} M citric acid, 7) 5×10^{-3} M PMA + 500×10^{-3} M citric acid) were made, transferred to a ceramic container, and were illuminated under UV light (365 nm). UV light was turned on and off and photos were taken. It could be observed that group 6 (5×10^{-3} M PMA + 300×10^{-3} M citric acid) was the most suitable for UV dosage measurement because it was the most sensitive with minimal raw material.

Color Change Comparison of PMA/Citric Acid and PMA/Lactic Acid Solutions under UV Illumination: Solution A (5×10^{-3} M PMA/ 300×10^{-3} M citric acid solution) and solution B (5×10^{-3} M PMA/ 300×10^{-3} M lactic acid solution) were prepared by dissolving stoichiometric materials in DI water. Two solutions were transferred to transparent plastic containers, UV light was turned on and off, and photos were taken.

Color Change Comparison of PMA/Citric Acid and PMA/Lactic Acid on a Piece of Filter Paper under UV Illumination: A drop of solution A (left) and a drop of solution B (right) were dripped on a piece of filter paper and the paper was dried in 60°C oven for 10 min. The dried filter paper was taken out. UVC light was turned on and off above the paper and photos were taken.

Color Change Recording of PMA/Citric Acid Solution: 5×10^{-3} M PMA/ 300×10^{-3} M citric acid solution was prepared by dissolving stoichiometric materials in DI water. The solution was transferred to a transparent plastic container for illumination. UV light was turned on and off and photos were taken when the accumulated UV dosages were 0, 50, 100, 150, 200, 250, 300, 450, 600, 1000, and 1500 J m^{-2} . The above practice was performed once for UVA, UVB, and UVC lights, respectively.

Color Change Recording of PMA/Citric Acid Solution on a Piece of Filter Paper: 5×10^{-3} M PMA/ 300×10^{-3} M citric acid solution was prepared by dissolving stoichiometric materials in DI water. The prepared solution was used as ink to paint patterns in a piece of filter paper with the help of swabs and toothpicks. A dot, a “U” pattern, and a “V” pattern were drawn for UVA, UVB, and UVC illuminations, respectively. After drawing, the filter paper was dried in 60°C oven for 10 min and then taken out. UV light was turned on and off above the paper and photos were taken when the accumulated UV dosages were 0, 50, 100, 150, 200, 250, 300, 450, 600, 1000, and 1500 J m^{-2} . The above practice was performed once for UVA, UVB, and UVC lights, respectively.

Synthesis of $\text{Sr}_2\text{Nb}_3\text{O}_{10}$ Nanosheets: The layered oxide was prepared by traditional solid calcination and liquid exfoliation. First, $\text{KSr}_2\text{Nb}_3\text{O}_{10}$ was synthesized by calcining K_2CO_3 (99.99%), SrCO_3 (99.9%), and Nb_2O_5 (99.99%), which were grounded for 0.5 h with molar ratio K:Sr:Nb = 1.2:2:3

at 1373 K for 10 h in air. The excessive K_2CO_3 was added to compensate for the loss due to volatilization of the alkali component at high temperature. Then, the K^+ in the obtained powder was replaced by protons by slow stirring the powder in 4 M HNO_3 solution for 4 days and the acid was changed every day. After proton exchange, the powder was washed 3 times with DI water by centrifugation and dried at 80 °C in oven. The proton-exchanged powder was dispersed in 50 mL of aqueous solution that contained an equimolar amount of tetrabutylammonium (prepared from 25% aqueous solution) and was shaken for 10 days. After washing 3 times with DI water, the $Sr_2Nb_3O_{10}$ nanosheet suspension was collected by centrifugation.

Fabrication of $Ag/Sr_2Nb_3O_{10}/Ag$ Photodetector: 2D $Sr_2Nb_3O_{10}$ nanosheets were spray-coated onto a piece of filter paper on a 150 °C hot plate and Ag paste was used as the electrodes to construct a metal–semiconductor–metal photodetector.

Fabrication of $Ag/ZnO/Ag$ Photodetector: Commercial ZnO nanoparticles (99.9%, 200 nm) were dissolved in DI water to form a 10 mg mL⁻¹ suspension. The ZnO suspension was then spray-coated onto a piece of filter paper on a 150 °C hot plate and Ag paste was used as the electrodes to construct a metal–semiconductor–metal photodetector.

Construction of the Integral Device: $Sr_2Nb_3O_{10}$ nanosheets (or ZnO) were spray-coated onto a filter paper on a 150 °C hot plate, while the center area of the paper was protected by a glass slide. PMA/citric acid photochromic solution was then used as ink to write a “UV” pattern on the blank center area. Ag paste was used as the electrodes to construct a metal–semiconductor–metal photodetector.

Supporting Information

Supporting Information is available from the Wiley Online Library or from the author.

Acknowledgements

S.C. and C.L.Z. contributed equally to this work. The work was supported by the National Key R&D Program of China (Grant Nos. 2018YFA0703700 and 2017YFA0204600), the National Natural Science Foundation of China (Grant Nos. 51872050 and 1201101405), the Ministry of Education Joint Fund for Equipment Pre-Research (Grant No. 6141A02033241), and the Science and Technology Commission of Shanghai Municipality (Grant Nos. 19520744300, 18520710800, and 18520744600). Part of the research was carried out in the Fudan Nanofabrication Laboratory.

Conflict of Interest

The authors declare no conflict of interest.

Data Availability Statement

Data sharing is not applicable to this article as no new data were created or analyzed in this study.

Keywords

dosage, photodetectors, simultaneous photodetector, UV intensity, wearable photodetector

Received: January 11, 2021
Published online: March 10, 2021

- [1] H. Chen, K. Liu, L. Hu, A. A. Al-Ghamdi, X. S. Fang, *Mater. Today* **2015**, *18*, 493.
- [2] I. V. Ivanov, T. Mappes, P. Schaupp, C. Lappe, S. Wahl, *J. Biophotonics* **2018**, *11*, 201700377.
- [3] F. P. Boscoe, M. J. Schymura, *BMC Cancer* **2006**, *6*, 264.
- [4] S. A. Marchitti, Y. Chen, D. C. Thompson, V. Vasilioiu, *Eye Contact Lens* **2011**, *37*, 206.
- [5] Y. Matsumura, H. N. Ananthaswamy, *Toxicol. Appl. Pharmacol.* **2004**, *195*, 298.
- [6] B. K. Armstrong, A. Krickler, *J. Photochem. Photobiol., B* **2001**, *63*, 8.
- [7] D. F. MacFarlane, C. A. Alonso, *Arch. Dermatol.* **2009**, *145*, 447.
- [8] J. Wang, A. S. Jeevarathinam, A. Jhunjhunwala, H. Ren, J. Lemaster, Y. Luo, D. P. Fenning, E. E. Fullerton, J. V. Jokerst, *Adv. Mater. Technol.* **2018**, *3*, 1800037.
- [9] E. C. Davidson, A. Kotikian, S. Li, J. Aizenberg, J. A. Lewis, *Adv. Mater.* **2020**, *32*, 1905682.
- [10] A. Stützer, L. M. Welp, M. Raabe, T. Sachsenberg, C. Kappert, A. Wulf, A. M. Lau, S. S. David, A. Chernev, K. Kramer, A. Politis, O. Kohlbacher, W. Fischle, H. Urlaub, *Nat. Commun.* **2020**, *11*, 5250.
- [11] C. Wang, W. D. Yang, D. Raciti, A. Bruma, R. Marx, A. Agrawal, R. Sharma, *Nat. Mater.* **2021**, <https://doi.org/10.1038/s41563-020-00851-x>.
- [12] H. Inagaki, A. Saito, H. Sugiyama, T. Okabayashi, S. Fujimoto, *Emerging Microbes Infect.* **2020**, *9*, 1744.
- [13] E. O. Polat, G. Mercier, I. Nikitskiy, E. Puma, T. Galan, S. Gupta, M. Montagut, J. J. Piqueras, M. Bouwens, T. Durduran, G. Konstantatos, S. Goossens, F. Koppens, *Sci. Adv.* **2019**, *5*, eaaw7846.
- [14] A. Dubey, R. Mishra, Y. Hsieh, C. Cheng, B. Wu, L. Chen, S. Gwo, T. Yen, *Adv. Sci.* **2020**, *7*, 2002274.
- [15] R. Zhao, N. Ma, K. Song, Y. Yang, *Adv. Funct. Mater.* **2020**, *30*, 1906232.
- [16] W. Zou, M. Sastry, J. J. Gooding, R. Ramanathan, V. Bansal, *Adv. Mater. Technol.* **2020**, *5*, 1901036.
- [17] M. Wang, P. Zeng, Z. Wang, M. Liu, *Adv. Sci.* **2020**, *7*, 1903662.
- [18] S. Cai, X. Xu, W. Yang, J. Chen, X. S. Fang, *Adv. Mater.* **2019**, *31*, 1808138.
- [19] M. Ahmadi, T. Wu, B. Hu, *Adv. Mater.* **2017**, *29*, 1605242.
- [20] C. Sa, X. Xu, X. Wu, J. Chen, C. Zuo, X. S. Fang, *J. Mater. Chem. C* **2019**, *7*, 13097.
- [21] X. Xu, J. Chen, S. Cai, Z. Long, Y. Zhang, L. Su, S. He, C. Tang, P. Liu, H. Peng, X. S. Fang, *Adv. Mater.* **2018**, *30*, 1803165.
- [22] L. Hu, J. Yan, M. Liao, H. Xiang, X. Gong, L. Zhang, X. S. Fang, *Adv. Mater.* **2012**, *24*, 2305.
- [23] Z. Q. Li, Z. L. Li, Z. F. Shi, X. S. Fang, *Adv. Funct. Mater.* **2020**, *30*, 2002634.
- [24] X. S. Fang, T. Zhai, U. K. Gautam, L. Li, L. Wu, Y. Bando, D. Golberg, *Prog. Mater. Sci.* **2011**, *56*, 175.
- [25] H. Dong, H. Zhu, Q. Meng, X. Gong, W. Hu, *Chem. Soc. Rev.* **2012**, *41*, 1754.
- [26] J. Zhang, Q. Zou, H. Tian, *Adv. Mater.* **2013**, *25*, 378.
- [27] J. Zhang, J. Wang, H. Tian, *Mater. Horizons* **2014**, *1*, 169.
- [28] Y. Ke, J. Chen, G. Lin, S. Wang, Y. Zhou, J. Yin, P. S. Lee, Y. Long, *Adv. Energy Mater.* **2019**, *9*, 1902066.
- [29] H. Tian, H. Y. Tu, *Adv. Mater.* **2000**, *12*, 1597.
- [30] R. Pardo, M. Zayat, D. Levy, *Chem. Soc. Rev.* **2011**, *40*, 672.
- [31] T. He, J. Yao, *J. Mater. Chem.* **2007**, *17*, 4547.
- [32] K. Adachi, M. Tokushige, K. Omata, S. Yamazaki, Y. Iwazaki, *ACS Appl. Mater. Interfaces* **2016**, *8*, 14019.
- [33] J. D. Compain, P. Deniard, R. Dessapt, A. Dolbecq, O. Oms, F. Sécheresse, J. Marrot, P. Mialane, *Chem. Commun.* **2010**, *46*, 7733.
- [34] H. Qiu, Z. Liu, Y. Yao, M. Herder, S. Hecht, P. Samori, *Adv. Mater.* **2020**, *32*, 1907903.

- [35] M. S. Wang, G. Xu, Z. J. Zhang, G. C. Guo, *Chem. Commun.* **2010**, 46, 361.
- [36] G. Naren, C. W. Hsu, S. Li, M. Morimoto, S. Tang, J. Hernando, G. Guirado, M. Irie, F. M. Raymo, H. Sundén, J. Andréasson, *Nat. Commun.* **2019**, *10*, 3996.
- [37] H. Kuroiwa, Y. Inagaki, K. Mutoh, J. Abe, *Adv. Mater.* **2019**, *31*, 1805661.
- [38] W. Zou, A. González, D. Jampaiah, R. Ramanathan, M. Taha, S. Walia, S. Sriram, M. Bhaskaran, J. M. Dominguez-Vera, V. Bansal, *Nat. Commun.* **2018**, *9*, 3743.
- [39] Y. Shi, M. Manco, D. Moyal, G. Huppert, H. Araki, A. Banks, H. Joshi, R. McKenzie, A. Seewald, G. Griffin, E. Sen-Gupta, D. Wright, P. Bastien, F. Valceschini, S. Seité, J. A. Wright, R. Ghaffari, J. Rogers, G. Balooch, R. M. Pielak, *PLoS One* **2018**, *13*, e0190233..
- [40] E. Papaconstantinou, *Chem. Soc. Rev.* **1989**, *18*, 1.
- [41] H. L. Kee, H. Tang, *Angew. Chem., Int. Ed.* **2013**, *30*, 34.
- [42] S. Li, Y. Zhang, W. Yang, H. Liu, X. S. Fang, *Adv. Mater.* **2020**, *32*, 1905443.
- [43] P. Yu, K. Hu, H. Chen, L. Zheng, X. S. Fang, *Adv. Funct. Mater.* **2017**, *27*, 1703166.